



Article

High-Quality Graphene-Based Tunable Absorber Based on Double-Side Coupled-Cavity Effect

Qiong Wang, Zhengbiao Ouyang *, Mi Lin and Yaoxian Zheng

THz Technical Research Center of Shenzhen University, Shenzhen Key Laboratory of Micro-Nano Photonic Information Technology, Key Laboratory of Optoelectronic Devices and Systems of Ministry of Education and Guangdong Province, College of Physics and Optoelectronic Engineering, Shenzhen University, Shenzhen 518060, China; qwang@szu.edu.cn (Q.W.); linfengas111@szu.edu.cn (M.L.); jewel5282@163.com (Y.Z.)

* Correspondence: zhouyang@szu.edu.cn

Abstract: Graphene-based devices have important applications attributed to their superior performance and flexible tunability in practice. In this paper, a new kind of absorber with monolayer graphene sandwiched between two layers of dielectric rings is proposed. Two peaks with almost complete absorption are realized. The mechanism is that the double-layer dielectric rings added to both sides of the graphene layer are equivalent to resonators, whose double-side coupled-cavity effect can make the incident electromagnetic wave highly localized in the upper and lower surfaces of graphene layer simultaneously, leading to significant enhancement in the absorption of graphene. Furthermore, the influence of geometrical parameters on absorption performance is investigated in detail. Also, the device can be actively manipulated after fabrication through varying the chemical potential of graphene. As a result, the frequency shifts of the two absorption peaks can reach as large as 2.82 THz/eV and 3.83 THz/eV, respectively. Such a device could be used as tunable absorbers and other functional devices, such as multichannel filters, chemical/biochemical modulators and sensors.



Citation: Wang, Q.; Ouyang, Z.; Lin, M.; Zheng, Y. High-Quality Graphene-Based Tunable Absorber Based on Double-Side Coupled-Cavity Effect. *Nanomaterials* **2021**, *11*, 2824. <https://doi.org/10.3390/nano11112824>

Academic Editors: Filippo Giannazzo and Philipp Braeuningger-Weimer

Received: 9 September 2021
Accepted: 20 October 2021
Published: 24 October 2021

Publisher's Note: MDPI stays neutral with regard to jurisdictional claims in published maps and institutional affiliations.



Copyright: © 2021 by the authors. Licensee MDPI, Basel, Switzerland. This article is an open access article distributed under the terms and conditions of the Creative Commons Attribution (CC BY) license (<https://creativecommons.org/licenses/by/4.0/>).

Keywords: graphene-based device; tunable absorber; coupled-cavity system; finite difference time domain

1. Introduction

Monolayer graphene, a semimetallic two-dimensional material of hexagonally arranged carbon atoms, has attracted significant attention due to its extraordinary mechanical, thermal, electronic, and optical properties. Similar to three-dimensional noble metal nanoparticles, monolayer graphene can also support surface plasmon-polaritons (SPPs), and it exhibits more remarkable properties such as flexible electrical tunability, strong light confinement, and relatively low ohmic losses [1–4]. Due to these unique characteristics, graphene-based absorbers, optical modulators, logic processors, power splitters, optical filters, and biochemical sensors have been realized [5–13].

Recently, great attention has been devoted to graphene-based absorbers. However, the absorption of monolayer graphene is very low. In order to solve this problem, some strategies have been proposed. For instance, high-efficiency absorbers have been realized by designing graphene patterns with different shapes, such as split ring, fishing-net and E-shaped models [14,15]. Another method is to use periodic metal units to excite surface plasmon polaritons to enhance the absorption of graphene [16–21]. In addition, periodic multi-layer dielectric materials have also been reported to enhance the absorption of graphene based on optical resonance effect [22–26]. These achievements open up a new way for designing graphene-based absorbers. However, in these approaches, no matter if adding periodic metal units or multi-layer dielectric materials to monolayer graphene, it needs a complicated fabrication process or it may give rise to a big size of device. Moreover, in these studies, only single-side coupled-cavity effect has been applied. These would bring

limitations to applications. Therefore, graphene-based absorbers with high-efficiency and ultra-compact structure are necessary to be further explored.

In this paper, in order to improve the absorption of monolayer graphene and simultaneously keep the size of device compact, a new kind of absorber with monolayer graphene sandwiched between two layers of dielectric rings is proposed. The double-layer dielectric rings equivalent to resonators that are symmetrically added to both sides of monolayer graphene. Due to the double-side coupled-cavity effect, almost complete absorption is obtained. The influence of geometrical parameters on absorption performance is further discussed in detail. Also, the result demonstrates that a wide frequency range of absorption spectrum could be tuned by varying the chemical potential of graphene. Such a device could be used as tunable absorbers and other functional devices, such as multichannel filters, chemical/biochemical modulators and sensors.

Here, there are two points need to be emphasized. Firstly, different from some research in which only single-side coupled-cavity structures have been investigated [27–29], the double-layer dielectric rings we proposed to add to both sides of monolayer graphene could be more efficient to enhance the electric-field intensities on the upper and lower surfaces of graphene, whose double-side coupled-cavity effect could increase the absorption of graphene. Secondly, the double-layer dielectric rings do not require fabrication of metallic nanostructures [30] and could make the size of device more compact, compared with the periodic metal units or multi-layer dielectric materials reported in the other articles. The use of dielectric rings shows advantages in terms of fabrication cost since they have a lower price.

2. Structure Design and Calculation Method

The schematic of graphene-based absorber we proposed is shown in Figure 1a. On an insulator substrate with refractive index $n_{\text{sub}} = 1.45$, monolayer graphene is sandwiched between two layers of identical dielectric-ring arrays. The dielectric is chosen as silicon with refractive index $n_{\text{silicon}} = 3.4$. The upper and lower layers of dielectric-ring arrays are symmetric with respect to the graphene plane. The lower layers of dielectric-ring arrays are embedded in polymethyl methacrylate (PMMA) layer with refractive index $n_{\text{PMMA}} = 1.48$. The thickness of the insulator substrate is set as $D_{\text{sub}} = 12 \mu\text{m}$. A gold layer is deposited at the back side of the insulator substrate to present any transmission through the structure. In this way, perfect absorption can be obtained when the reflection is close to zero. The structure is periodic in the x -axis and the y -axis directions with periodic constant $P = 8.5 \mu\text{m}$. Figure 1b shows the simulation model of a pair of dielectric rings. Figure 1c shows the x - y cross section of a single dielectric ring. The inner and outer radii of dielectric ring are assumed as $R_{\text{in}} = 1.4 \mu\text{m}$ and $R_{\text{out}} = 2.4 \mu\text{m}$, respectively. The height is set as $H_{\text{ring}} = 3 \mu\text{m}$. The PMMA layer has the same thickness $H_{\text{PMMA}} = H_{\text{ring}} = 3 \mu\text{m}$. For convenience in the following analysis, a new parameter $W_{\text{ring}} = R_{\text{out}} - R_{\text{in}}$ standing for the width of the dielectric rings is defined.

For the structure, monolayer graphene is modeled as a conductive surface with thickness $D_g = 0.35 \text{ nm}$ in the simulations. The surface conductivity $\sigma(\omega, \mu_c, \Gamma, T)$ in THz range can be expressed by the Drude model according to the Kubo formula, as given by [15],

$$\sigma(\omega, \mu_c, \Gamma, T) = \frac{e^2 \kappa_B T \tau}{\pi \hbar^2 (1 + j\omega\tau)} \left\{ \frac{\mu_c}{\kappa_B T} + 2 \ln \left[\exp\left(-\frac{\mu_c}{\kappa_B T}\right) + 1 \right] \right\} \quad (1)$$

where ω is the radian frequency, μ_c is the chemical potential of graphene, $\Gamma = (2\tau)^{-1}$ is the phenomenological scattering rate with τ standing for the relaxation time due to charge carrier scattering, T is the temperature, \hbar is the reduced Plank constant, κ_B is the Boltzmann constant, e is the electron charge. The relaxation time satisfies the relationship $\tau = \mu \mu_c / e v_F^2$. Here, $v_F = 10^6 \text{ m/s}$ represents the Fermi velocity and μ is the carrier mobility of graphene. According to reported result, μ can be changed and the value as high as $4 \text{ m}^2/\text{Vs}$ can be obtained at room temperature [31]. Different μ_c is obtained by changing the dc voltage bias.

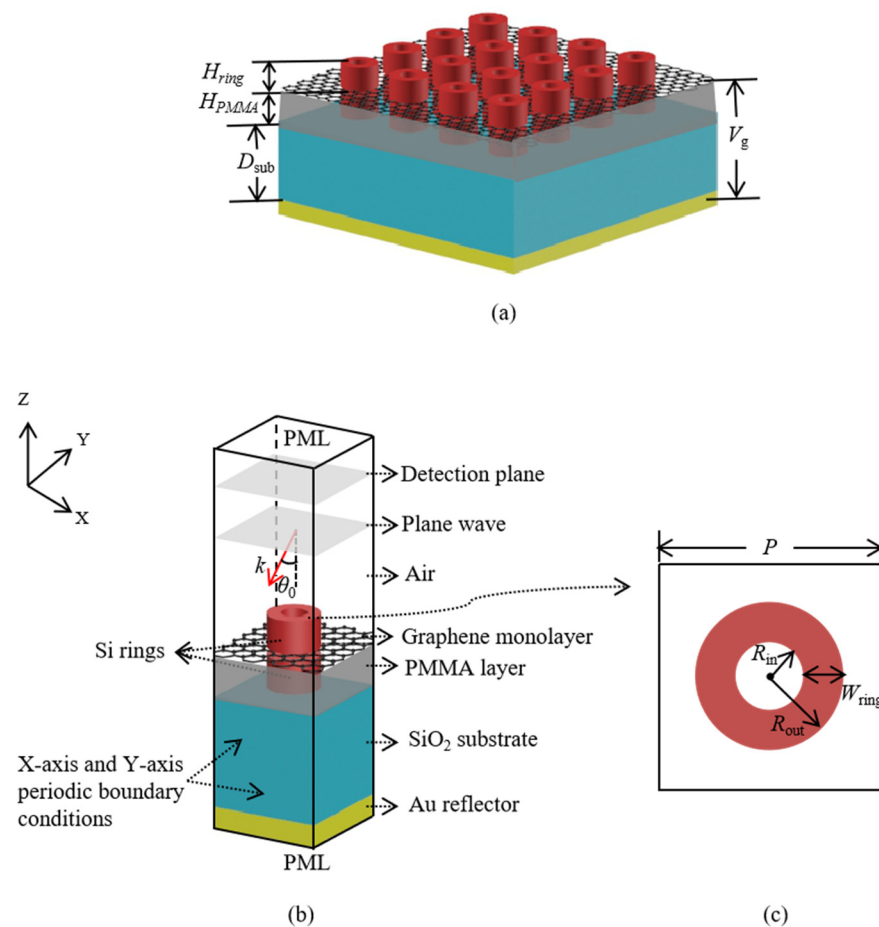


Figure 1. (a) The schematic of three-dimensional graphene-based absorber with monolayer graphene sandwiched between two layers of dielectric rings; (b) the simulation model of a pair of dielectric rings; (c) the x-y cross section of a single dielectric ring.

In the calculation, the finite difference time domain (FDTD) method is employed to calculate the reflection properties and simulate the electromagnetic field distributions of structure. As shown in Figure 1b, periodic boundary conditions are applied in both x -axis and y -axis directions to simulate the periodic structure. Perfectly matched layers (PMLs) are used at the outside of the top and bottom planes of calculation space to absorb the electromagnetic wave. In x - z plane, θ_0 represents incident angle. When the incident electromagnetic wave reaches the gold layer, it is completely reflected if the thickness of gold substrate is set large enough. Therefore, the transmission is zero. The absorption of structure is calculated by $A = 1 - R$ with $R = P_{re}/P_{in}$, in which P_{in} and P_{re} stand for the input and reflection energy flows, respectively. P_{re} is detected at the back of incident wave plane.

3. Results and Discussions

In Figure 2a, it gives the absorption spectrum of the proposed graphene-based structure, as shown by the black line. For the parameters, $T = 300$ K, $\tau = 1$ ps, $\mu_c = 1.0$ eV and $\mu = 1$ m²/Vs are chosen. The period unit for calculating is given in the inset. Here, Under TE-polarized normal incident wave (TE wave, the electric field along x -axis direction), it can be seen that there are two obvious absorption peaks at $f_1 = 5.18$ THz and $f_2 = 7.02$ THz. For convenience, they are denoted as modes M_1 and M_2 , respectively. The two peaks exhibit ultra-high absorption, reaching to 98.6% and 99.8%, respectively. In order to explore this absorption phenomenon, the electric-field amplitude distributions corresponding to the two absorption peaks are simulated and shown in Figure 2b–e. Figure 2b,c represent the electric-field amplitude distributions of mode M_1 at the x - z plane ($y = 0$) and x - y plane

($z = 0$), respectively, and Figure 2d,e represent that of mode M_2 . It can be observed that the electric-field amplitude distributions of modes M_1 and M_2 are highly localized at the interfaces of the upper-layer dielectric rings and graphene layer, and the lower-layer dielectric rings and graphene layer. Not only that, there are also strong electric-field amplitude distributions localized in the inner space of the double-layer dielectric rings. As shown in Figure 2f, the double-layer dielectric rings added on both sides of the graphene layer are equivalent to double-side coupled-cavity model. For modes M_1 and M_2 , the electric-field intensities of the upper and lower graphene interfaces are simultaneously enhanced by the resonance of double-side coupled cavities, which reinforces the graphene-wave interaction and enhances the absorption of graphene layer. On the other hand, referring to the literature [32], when the relaxation time of graphene is reduced to $\tau = 0.05$ ps ($\mu_c = 0.5$ eV), the absorption spectrum is also calculated, as shown by the green line in Figure 2a. We can see that the absorption is reduced due to the decrease in the corresponding conductivity of graphene.

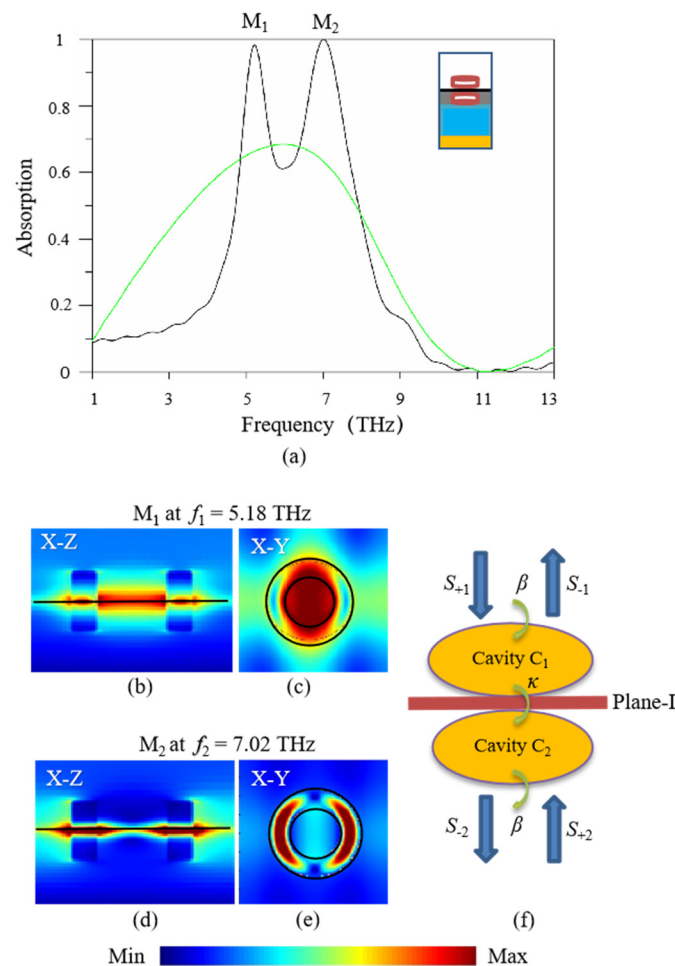


Figure 2. (a) The absorption spectrum of the proposed absorber with monolayer graphene sandwiched between two layers of dielectric rings, black line for $\tau = 1$ ps and green line for $\tau = 0.05$ ps, and its electric-field amplitude distributions at the absorption peaks for $\tau = 1$ ps, (b,c) for mode M_1 at $f_1 = 5.18$ THz, (d,e) for mode M_2 at $f_2 = 7.02$ THz, and (f) the equivalent double-side coupled-cavity model.

In order to further explain the numerical results above, the absorption performance based on the double-side coupled-cavity effect is also investigated by coupled mode theory (CMT) [23]. According to the simulation model of a single-period of the proposed graphene-based structure in Figure 1b, the upper-layer and lower-layer dielectric rings

are respectively denoted as cavity C_1 and cavity C_2 , and the unit cell of graphene layer is denoted as plane-I. Cavity C_1 and cavity C_2 are symmetric related to plane-I. The model of plane-I coupled with cavity C_1 and cavity C_2 can be considered as a coupled-cavity system, as shown in Figure 2f, which also can be described by the following formula based on the CMT analysis [33,34].

$$\frac{da_1}{dt} = (j\omega_1 - \beta_1)a_1 + \sqrt{2\beta_1}S_{+1} - j\kappa a_2 \quad (2)$$

$$\frac{da_2}{dt} = (j\omega_2 - \beta_2)a_2 + \sqrt{2\beta_2}S_{+2} - j\kappa a_1 \quad (3)$$

$$S_{-1} = -S_{+1} + j\sqrt{2\beta_1}a_1 \quad (4)$$

where a_i ($i = 1, 2$) is the mode amplitude of cavity C_i , ω_i ($i = 1, 2$) is the resonance frequency of cavity C_i , S_{+i} and S_{-i} are the amplitudes of the incoming and the outgoing waves for cavity C_i , respectively, and κ is the mutual coupling coefficient between the two cavities C_1 and C_2 , β_i is the coupling coefficient between cavity C_i and free space. We have $\omega_1 = \omega_2$ and $\beta_1 = \beta_2$ if considering the symmetry in structure, so new symbols $\omega_0 = \omega_1 = \omega_2$ and $\beta = \beta_1 = \beta_2$ are defined. In our case, it has $S_{+2} = 0$. Assuming that $S_{\pm i}$ and a_i ($i = 1, 2$) have time dependence $\exp(j\omega t)$, we can obtain the following relation from Equation (3):

$$\frac{a_2}{a_1} = \frac{-j\kappa}{j\omega - j\omega_0 + \beta} \quad (5)$$

From Equations (2), (4) and (5), the absorption of structure can be calculated as:

$$A = 1 - \left| \frac{S_{-1}}{S_{+1}} \right|^2 = 1 - \left| \frac{(j\omega - j\omega_0 + \beta)^2 + \kappa^2 - 2\beta\kappa}{(j\omega - j\omega_0 + \beta)^2 + \kappa^2} \right|^2 \quad (6)$$

As can be observed from Equation (6), at resonance frequency ($\omega = \omega_0$), if β is equal to κ , perfect absorption occurs. This critical coupling condition suggests that the impedance matching between cavities C_1 and C_2 must be equal to that between cavity C_1 (or cavity C_2) and free space. When the incident wave is chosen at the resonance frequency ($\omega = \omega_0$) and the system satisfies critical coupling condition ($\beta = \kappa$), resonant modes are excited at the interface of the upper-layer dielectric ring and graphene layer (called upper-layer resonant mode), and simultaneously excited at the interface of the lower-layer dielectric ring and graphene layer (called lower-layer resonant mode), as can be shown by the electric-field amplitude distributions of modes M_1 and M_2 in Figure 2b,d. The upper-layer and lower-layer resonant mode distributions are symmetric related to the graphene layer due to the high symmetry in structure. Based on the coupled-cavity effect, electric field intensity around the monolayer graphene is enhanced, which reinforces the graphene-wave interaction. As a result, the reflection wave of structure nearly vanishes and almost all the incident energies are absorbed. Perfect absorption occurs.

For comparison, two relatively simple structures are considered, one is the structure only with the upper-layer dielectric rings (called simple structure 1), and the other is the structure only with the lower-layer dielectric rings (called simple structure 2). Their absorption spectra are plotted in Figure 3a, with the periodic units for calculating are given in the left and right insets, respectively. It shows that only one high-absorption peak appears for a single spectrum line, i.e., $f_{up} = 6.22$ THz for simple structure 1 (see blue line) with absorption 75.5%, denoted as M_{up} , and $f_{down} = 9.44$ THz for simple structure 2 (see red line) with absorption 85.6%, denoted as M_{down} . For mode M_{up} , its electric-field amplitude distributions in Figure 3b,c show that there are strong field distributions at the interface of the upper-layer dielectric rings and graphene layer, and also at the inner space of the upper-layer dielectric rings. The upper-layer dielectric rings are equivalent to single-side resonance cavities added above the graphene layer, as shown in Figure 3d. On the other hand, for mode M_{down} , its electric-field amplitude distributions in Figure 3e,f show

that there are strong field distributions at the lower-layer dielectric rings and graphene layer. The lower-layer dielectric rings are equivalent to resonance cavities added below the graphene layer, as shown in Figure 3g. Comparing Figure 2 with Figure 3, we conclude that the absorption spectrum (black line) in Figure 2a is approximately a combination of the coupled effect of simple structures 1 (only with the upper-layer dielectric rings) and simple structures 2 (only with the lower-layer dielectric rings). The double-layer dielectric rings added on both sides of graphene layer can bring higher absorption efficiency than that of only adding a single layer of dielectric rings on one side of the graphene layer, which is because a double-side coupled-cavity model can yield stronger resonance effect than a single-side-cavity model.

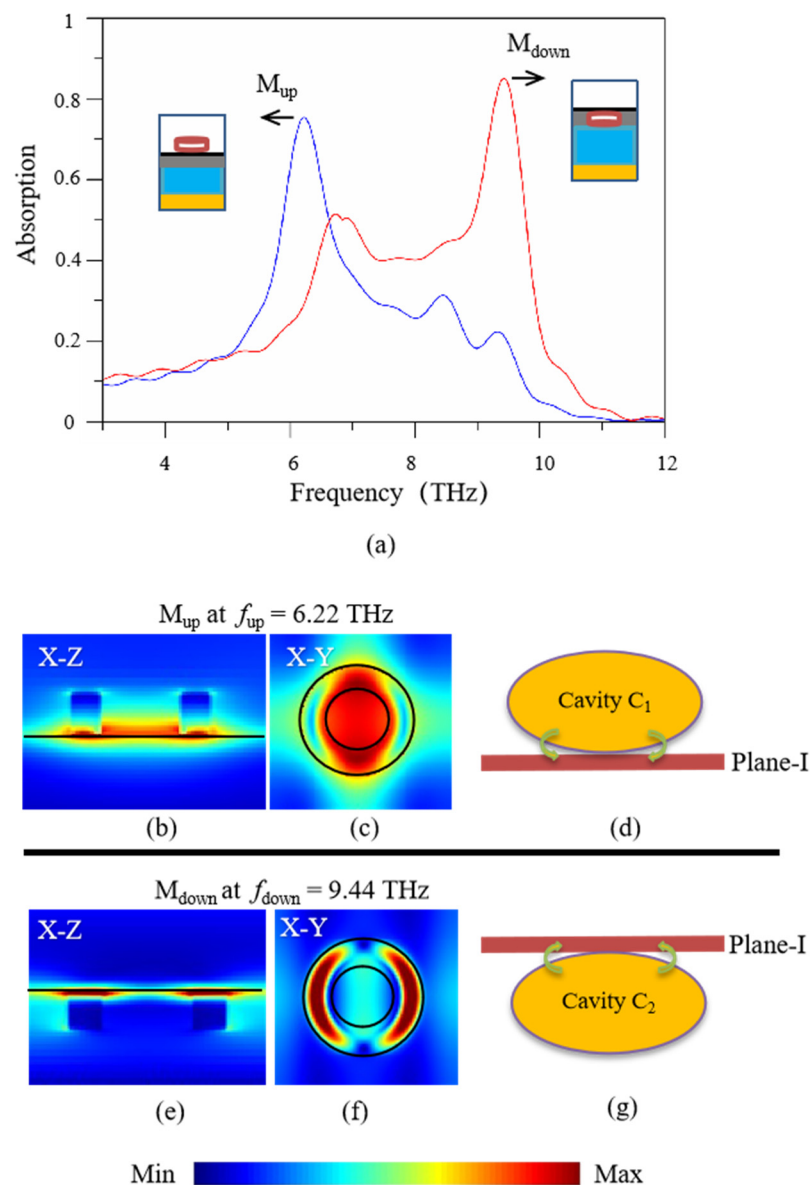


Figure 3. (a) The absorption spectra of simple structure 1 only with a single layer of dielectric rings added above the graphene layer (blue line) and simple structure 2 only with a single layer of dielectric rings added below the graphene layer (red line), and (b,c) the electric-field amplitude distributions at the absorption peak M_{up} of simple structure 1 with $f_{up} = 6.22$ THz, and (d) the equivalent single-cavity-above-graphene model; (e,f) the electric-field amplitude distributions at the absorption peak M_{down} of simple structure 2 with $f_{down} = 9.44$ THz, and (g) the equivalent single-cavity-below-graphene model.

In addition, the influence of the geometrical parameters (W_{ring} , H_{ring} in Figure 1) on the absorption performance are investigated. These analyses provide some guidance to structural design and fabrication.

First, we investigate the influence of the width W_{ring} of the double-layer dielectric rings on the absorption performance. In Figure 4, it shows the change of absorption spectrum with the increase of W_{ring} . We observe that when W_{ring} is relatively small, such as $W_{ring} = 0.3 \mu\text{m}$, there is only one absorption peak at 8.91 THz with absorption 87.7%. As W_{ring} increases, two absorption peaks appear. It shows that when $W_{ring} = 1.0 \mu\text{m}$, two absorption peaks appear at 5.18 THz with absorption 98.6%, and 7.02 THz with absorption 99.8%, respectively. When W_{ring} further increases, the number of absorption peaks continues to increase. For instance, when $W_{ring} = 2.6 \mu\text{m}$, five high-absorption peaks appear at 3.56 THz with absorption 95.5%, 4.42 THz with absorption 99.8%, 5.49 THz with absorption 95.5%, 6.24 THz with absorption 96.6%, and 7.15 THz with absorption 83.3%, respectively. For this case, the frequency range of absorption above 75% is from 3.35 THz to 7.22 THz, while that for the case of $W_{ring} = 0.3 \mu\text{m}$ is only from 8.69 THz to 9.14 THz. It means that the absorption band is greatly widened when W_{ring} increases. This is because the relatively wide dielectric rings could bring an increase in contact area of the dielectric rings and graphene layer, then more resonance mode can be supported. The result also can be illustrated from the electric-field amplitude distributions of the absorption peaks for different W_{ring} , as shown in Figure 4g–l. The characteristic provides a significant design guide for developing graphene-based absorbers with multiple resonance peaks.

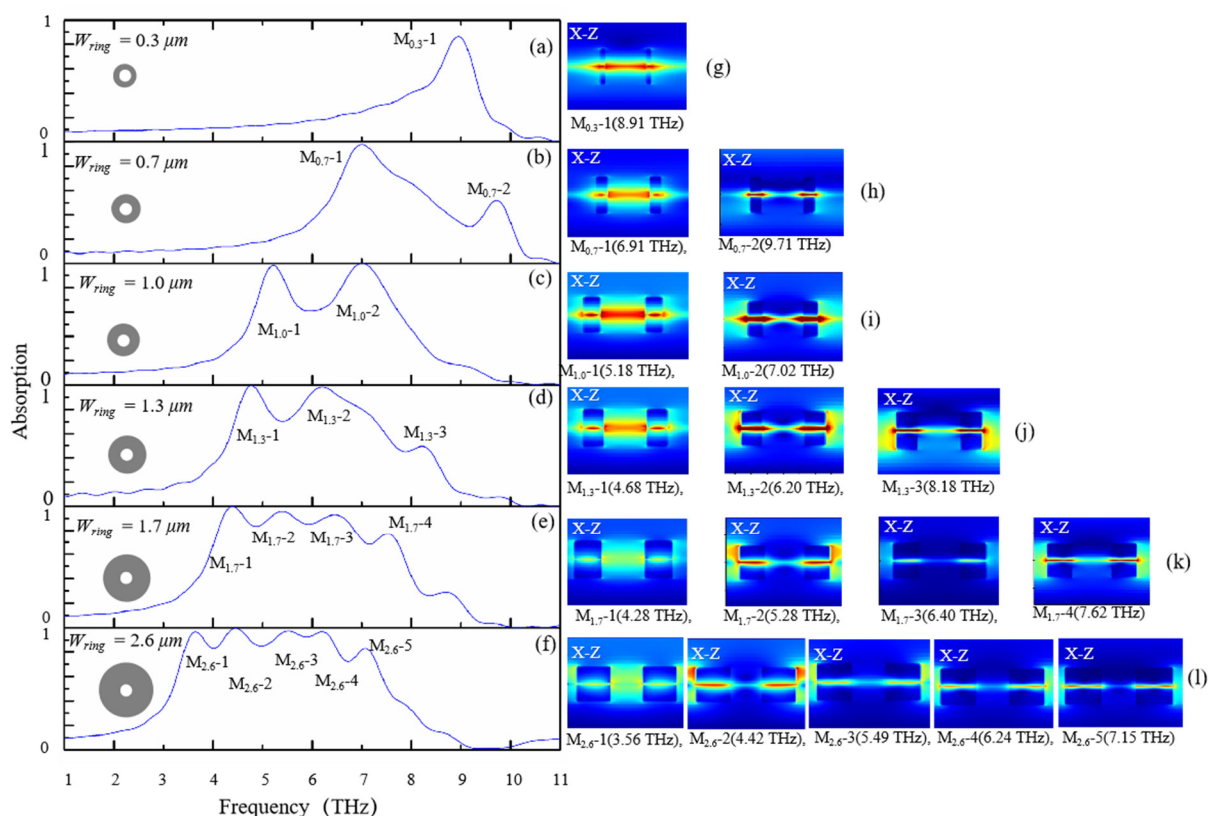


Figure 4. The absorption spectrum of the proposed graphene-based absorber when changing the width W_{ring} of dielectric rings, (a) $W_{ring} = 0.3 \mu\text{m}$, (b) $W_{ring} = 0.7 \mu\text{m}$, (c) $W_{ring} = 1.0 \mu\text{m}$, (d) $W_{ring} = 1.3 \mu\text{m}$, (e) $W_{ring} = 1.7 \mu\text{m}$, (f) $W_{ring} = 2.6 \mu\text{m}$, and (g–l) standing for electric-field amplitude distributions of the absorption peaks.

Next, the influence of the height H_{ring} of the dielectric rings on the absorption performance is investigated. We chose the parameter $W_{ring} = 1.0 \mu\text{m}$, referring to Figure 4c with two absorption peaks $M_{1,0-1}$ and $M_{1,0-2}$. Here, $M_{1,0-1}$ and $M_{1,0-2}$ are simplified as

M_1 and M_2 , respectively. As shown in Figure 5, when H_{ring} is relatively small, such as $H_{ring} = 0.8 \mu\text{m}$, the absorptions are 88.6% at 6.37 THz for the left mode M_1 , and 97.4% at 6.99 THz for the right mode M_2 . We can see that the absorptions are not high enough, which is because the dielectric rings with small height exhibit weak ability in z-direction spatial localization of electromagnetic wave (concluded from the comparison of Figure 5b–e), resulting in relatively weak resonance effect and unable to obtain enough strong absorption of graphene. When H_{ring} further increases, the absorption peaks M_1 has a red shift and the absorption peaks M_2 has no obvious change in frequency. Their absorptions are gradually enhanced. When $H_{ring} \geq 3.0 \mu\text{m}$, the two absorption peaks tend to be stable not only in frequency position, but also in absorption amplitude. The positions are basically fixed at about 5.18 THz for M_1 , and about 7.02 THz for M_2 . Moreover, the absorptions are above 98.5% for M_1 , and above 99.7% for M_2 . Therefore, $3.0 \mu\text{m} \leq H_{ring} \leq 5.0 \mu\text{m}$ is the best range since H_{ring} being too small ($H_{ring} < 3.0 \mu\text{m}$) is not of avail to the localization of electromagnetic wave, and an H_{ring} too large ($H_{ring} > 5.0 \mu\text{m}$) is not necessary for fabrication in practice.

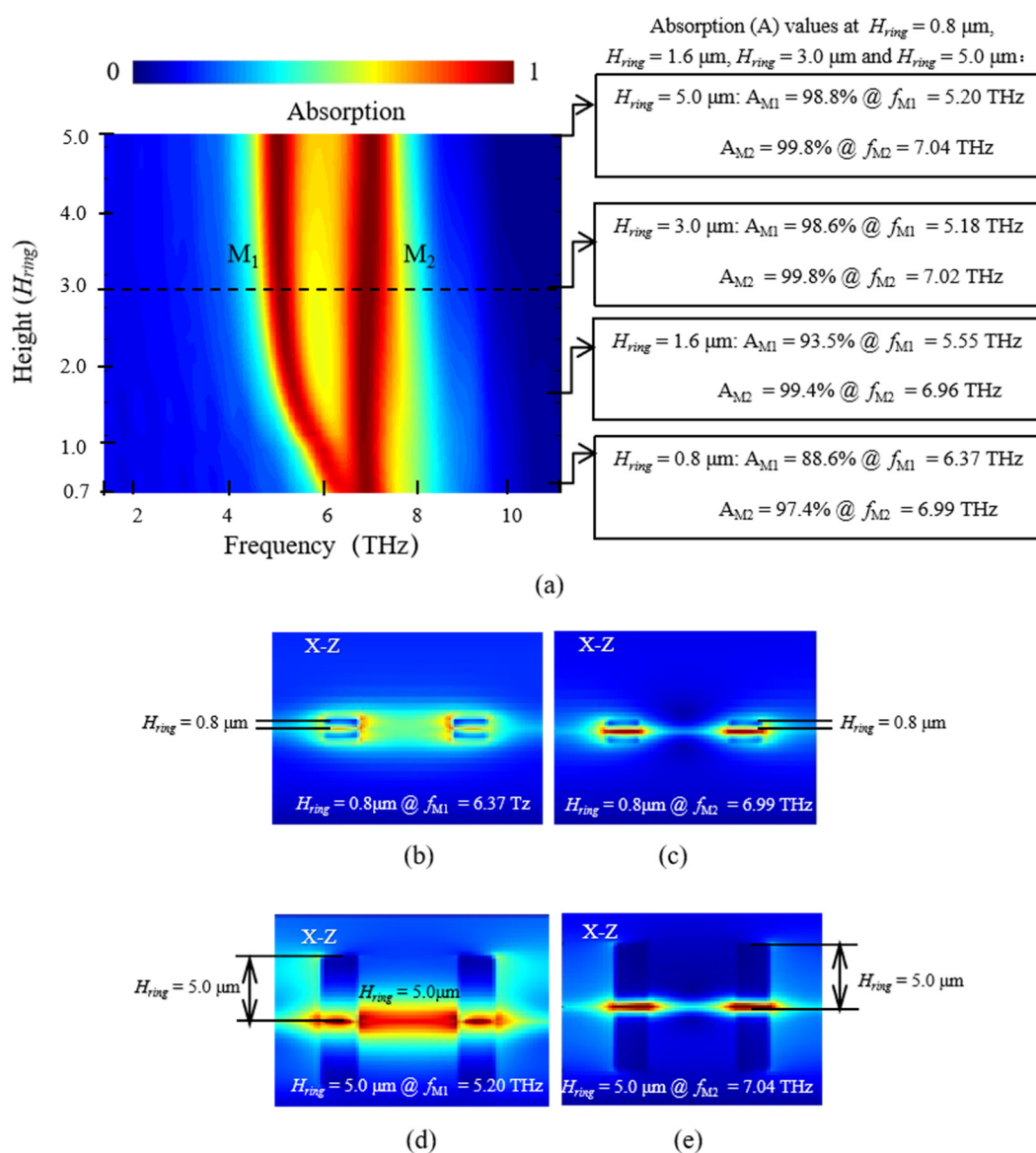


Figure 5. (a) The change of absorption of the proposed graphene-based absorber for different H_{ring} , and the electric-field amplitude distributions of (b) $H_{ring} = 0.8 \mu\text{m}$ for M_1 , (c) $H_{ring} = 0.8 \mu\text{m}$ for M_2 , (d) $H_{ring} = 5.0 \mu\text{m}$ for M_1 , and (e) $H_{ring} = 5.0 \mu\text{m}$ for M_2 .

On the other hand, one remarkable advantage of graphene is that its chemical potential μ_c can be manipulated over a wide range through adjusting direct-current bias voltage V_g that is added between the graphene layer and gold substrate. Due to this characteristic, graphene-based devices can be actively manipulated after final design and fabrication. As shown in Figure 6, it illustrates the influence of changing the chemical potential μ_c of graphene on absorption performance. The parameters $W_{ring} = 1.0 \mu\text{m}$, $H_{ring} = 3.0 \mu\text{m}$ are chosen, referring to Figures 4 and 5. In this case, two absorption peaks M_1 and M_2 can be observed. In Figure 6, it shows that when μ_c increases from 0.1 eV to 1.5 eV ($\mu = 1 \text{ m}^2/\text{Vs}$), both of the two absorption peaks M_1 and M_2 exhibit obvious blue shifts and the frequency shifts can reach as large as 2.82 THz/eV for the left peak M_1 and 3.83 THz/eV for the right peak M_2 , which demonstrates the remarkable tunability of structure. Meanwhile, when μ_c increases from 0.1 eV to 1.5 eV, the absorption of the left peak M_1 increases from 12.6% to 98.8%, and that of the right peak M_2 also increases from 10.7% to 99.8%. It indicates that the absorptions of the two peaks are enhanced with the increase of μ_c . Such a characteristic could be used as tunable absorbers and other functional devices, such as multichannel filters, chemical/biochemical modulators and sensors.

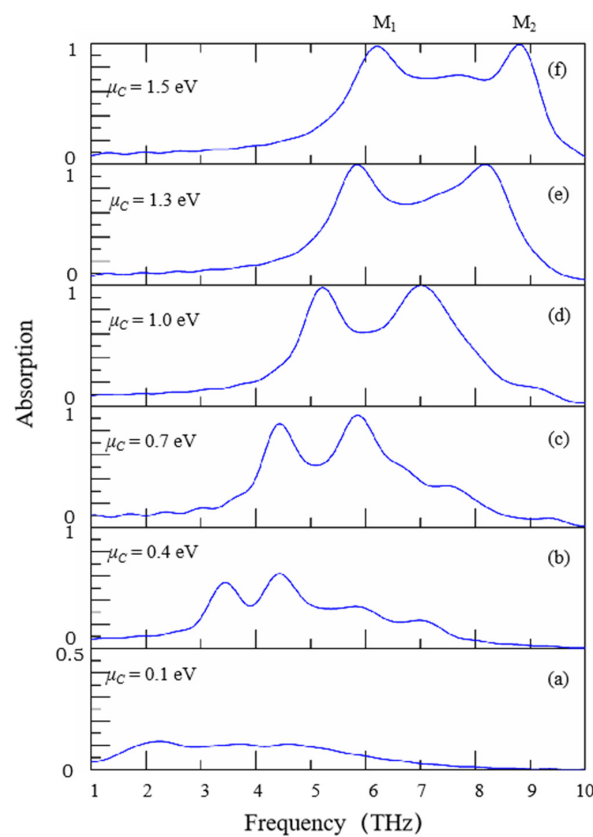


Figure 6. (a) The absorption spectra of the proposed graphene absorber for different μ_c , (a) $\mu_c = 0.1 \text{ eV}$, (b) $\mu_c = 0.4 \text{ eV}$, (c) $\mu_c = 0.7 \text{ eV}$, (d) $\mu_c = 1.0 \text{ eV}$, (e) $\mu_c = 1.3 \text{ eV}$ and (f) $\mu_c = 1.5 \text{ eV}$. μ_c is the chemical potential of graphene.

The frequency spectra of the absorption are represented in Figure 6 for different values of chemical potential obtained by increasing the dc voltage bias. The dielectric breakdown strength of the used materials is relatively high (large than $20 \text{ V}/\mu\text{m}$) in theory, which can satisfy the need of design. In practice, a layer of ionic gel would be applied over graphene layer. It can significantly reduce the voltage bias and avoid dielectric break down. This method has been demonstrated in the reference [35].

In the discussions above, absorption spectra have been investigated for normal incidence ($\theta_0 = 0^\circ$). Finally, the absorption spectra at different θ_0 are illustrated for TE and TM

polarizations, as shown in Figure 7a,b, respectively. When the plane of incidence is set in the x-z plane, the incident angle θ_0 is defined as the angle between the incident plane wave and the positive z-direction, as shown in Figure 1b. According to refraction theory, we have,

$$n_0 \sin \theta_0 = n_1 \sin \theta_1 \quad (7)$$

where n_0 is the refractive index of air, n_1 is the effective refractive index of absorption domain and θ_1 is the refraction angle. Here, n_1 is complex due to the absorption. We can define $n_1 = n_{1r} + i \cdot n_{1i}$, where n_{1r} and n_{1i} are the real and imaginary components of n_1 . Therefore, the refraction angle θ_1 is also complex. It can be expressed as $\theta_1 = \theta_{1r} + i \cdot \theta_{1i}$, where θ_{1r} and θ_{1i} are the real and imaginary components of θ_1 . Therefore, the complex refraction angle θ_1 is related to the parameters θ_0 , n_0 , n_{1r} and n_{1i} . With FDTD Solutions software, the simulation model can be calculated by setting the parameters θ_0 , n_0 , n_{1r} and n_{1i} , in which n_0 , n_{1r} and n_{1i} depend on the parameters of graphene and dielectric materials. It should be noted that the refracted plane wave into the absorber is nonuniform since it is closely related to the corresponding material in the refraction region. The absorption of structure can be indirectly calculated by collecting the total reflection energy flow at the detection plane, as shown in Figure 1b. In Figure 7, we can find that the absorption peaks M_1 and M_2 are almost unchanged at incident angles as large as 35° for TE polarization and 45° for TM polarization. This phenomenon is attributed to the high symmetry in the structure. The results would have important applications for wide-angle absorbers in practice.

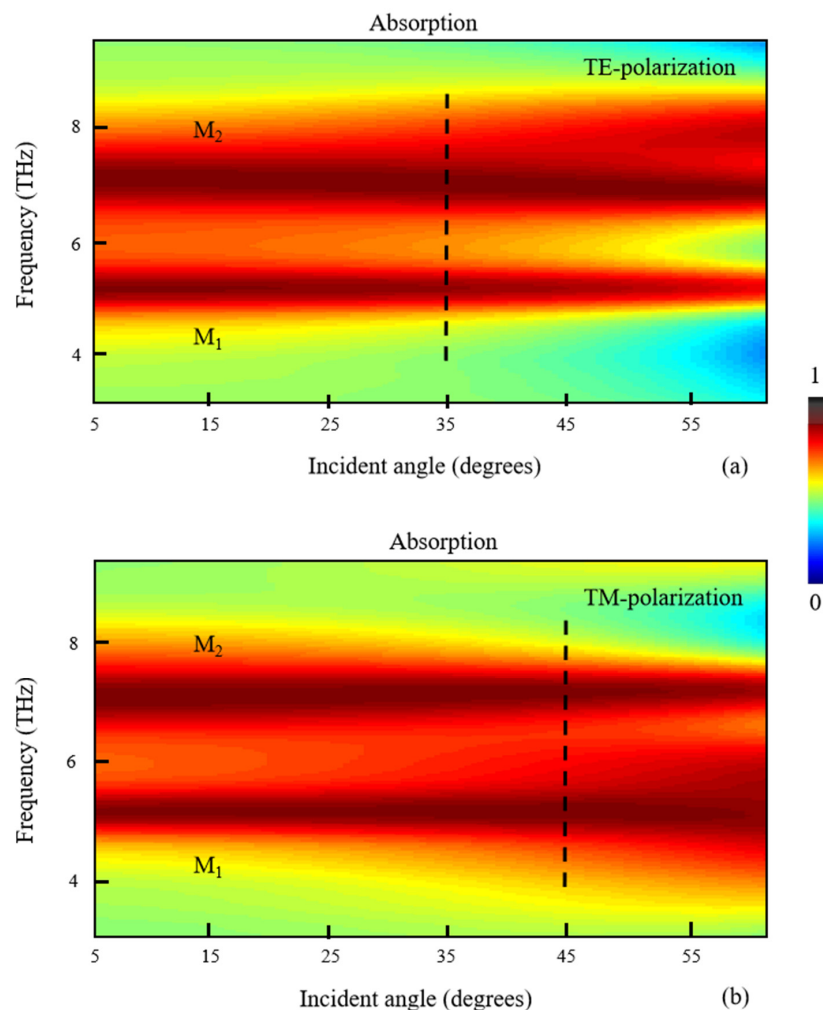


Figure 7. The effect of incident angle θ_0 on absorption when the incident wave is chosen as (a) TE polarization and (b) TM polarization.

4. Conclusions

In summary, we introduce a new kind of high-quality graphene-based absorber using a double-side coupled-cavity effect. In this structure, monolayer graphene is sandwiched between two layers of dielectric rings, which are equivalent to resonators coupled to both sides of graphene layer. The double-side coupled-cavity effect can greatly enhance the absorption of graphene. The result shows that two peaks with almost complete absorption are obtained. The influence of geometrical parameters on absorption performance are investigated in detail. Furthermore, through varying the chemical potential of graphene, the frequency shifts of the two absorption peaks can reach as large as 2.82 THz/eV and 3.83 THz/eV, respectively. The proposed structure also could be used for applications related to multichannel filters, chemical/biochemical modulators and sensors.

Author Contributions: Q.W. designed the structure and wrote the paper; M.L. analyzed the theory; Y.Z. performed the simulations; Z.O. revised the paper. All authors have read and agreed to the published version of the manuscript.

Funding: This work was supported by the Shenzhen Science and Technology Project (JCYJ20190808161801637, JCYJ20180305124247521, JCYJ20190808151017218), National Natural Science Foundation of China (NSFC) (61605128), and Guangdong Province Natural Science Funds (GDNSF) (2020A1515011154).

Institutional Review Board Statement: Not applicable.

Informed Consent Statement: Not applicable.

Data Availability Statement: The data presented in this study are available on request from the corresponding author.

Conflicts of Interest: The authors declare no conflict of interest.

References

1. Li, H.; Yu, J. Bifunctional terahertz absorber with a tunable and switchable property between broadband and dual-band. *Opt. Express* **2020**, *28*, 25225–25237. [[CrossRef](#)]
2. Ju, Z.Z.; Deng, M.; Wang, J.; Chen, L. Reconfigurable multifrequency and wide-angle directional beaming of light from a subwavelength metal slit with graphene metasurfaces. *Opt. Lett.* **2020**, *45*, 2882–2885. [[CrossRef](#)]
3. Wang, Y.P.; You, J.W.; Lan, Z.H.; Panoiu, N.C. Topological valley plasmon transport in bilayer graphene metasurfaces for sensing applications. *Opt. Lett.* **2020**, *45*, 3151–3154. [[CrossRef](#)]
4. Heidari, M.; Ahmadi, V. Graphene-based mid-infrared plasmonic isolator with multimode interferometer. *Opt. Lett.* **2020**, *45*, 5764–5767. [[CrossRef](#)]
5. Shi, S.F.; Zeng, B.; Han, H.L.; Hong, X.; Tsai, H.Z.; Jung, H.S.; Zett, A.; Crommie, M.F.; Wang, F. Optimizing broadband terahertz modulation with hybrid graphene/metasurface structures. *Nano Lett.* **2015**, *15*, 372–377. [[CrossRef](#)]
6. Gao, F.; Zhu, Z.H.; Xu, W.; Zhang, J.F.; Guo, C.C.; Liu, K.; Yuan, X.D.; Qin, S.Q. Broadband wave absorption in single-layered and nanostructured graphene based on far-field interaction effect. *Opt. Express* **2017**, *25*, 9579–9586. [[CrossRef](#)]
7. Fan, Y.S.; Guo, C.C.; Zhu, Z.H.; Xu, W.; Wu, F.; Yuan, X.D.; Qin, S.Q. Monolayer-graphene-based perfect absorption structures in the near infrared. *Opt. Express* **2017**, *25*, 13079–13086. [[CrossRef](#)]
8. Yan, Z.D.; Zhu, Q.; Wan, M.J.; Lu, X.; Pu, X.T.; Tang, C.J.; Yu, L.L. Graphene ultraviolet ultrahigh-Q perfect absorption for nanoscale optical sensing. *Opt. Express* **2020**, *28*, 6095–6101. [[CrossRef](#)]
9. Yang, J.W.; Zhu, Z.H.; Zhang, J.F.; Guo, C.C.; Xu, W.; Liu, K.; Yuan, X.D.; Qin, S.Q. Broadband terahertz absorber based on multi-band continuous plasmon resonances in geometrically gradient dielectric-loaded graphene plasmon structure. *Sci. Rep.* **2018**, *8*, 3239. [[CrossRef](#)]
10. Hao, Q.Q.; Guo, J.; Yin, L.Y.; Ning, T.Y.; Ge, Y.Q.; Liu, J. Watt-level ultrafast bulk laser with a graphdiyne saturable absorber mirror. *Opt. Lett.* **2020**, *45*, 5554–5557. [[CrossRef](#)]
11. Jeong, S.Y.; Lee, J.U.; Hong, S.M.; Lee, C.W.; Hwang, S.H.; Cho, S.C.; Shin, B.S. Highly skin-conformal laser-induced graphene-based human motion monitoring sensor. *Nanomaterials* **2021**, *11*, 951. [[CrossRef](#)]
12. Guo, H.; Zhang, R.Z.; Li, H.; Wang, X.Y.; Lu, H.L.; Qian, K.; Li, G.; Huang, L.; Lin, X.; Zhang, Y.Y.; et al. Sizable band gap in epitaxial bilayer graphene induced by silicene intercalation. *Nano Lett.* **2020**, *20*, 2674–2680. [[CrossRef](#)]
13. Fan, X.; Wang, Q.; Zhou, M.; Liu, F.; Shen, H.; Wei, Z.; Wang, F.; Tan, C.; Meng, H. Humidity sensor based on a grapheme oxide-coated few-mode fiber Mach-Zehnder interferometer. *Opt. Express* **2020**, *28*, 24682–24692. [[CrossRef](#)]
14. Andryieuski, A.; Lavrinenko, A.V. Graphene metamaterials based tunable terahertz absorber: Effective surface conductivity approach. *Opt. Express* **2013**, *21*, 9144–9155. [[CrossRef](#)]

15. Han, J.Z.; Chen, R.S. Tunable broadband terahertz absorber based on a single-layer graphene metasurface. *Opt. Express* **2020**, *28*, 30289. [[CrossRef](#)]
16. Mirnia, S.E.; Lail, B.A. Dynamically tunable reflecting near-infrared bandpass filter based on a hybrid graphene–nanometallic structure. *Appl. Optics* **2020**, *59*, 5608–5614. [[CrossRef](#)]
17. Degl’Innocenti, R.; Jessop, D.S.; Shah, Y.D.; Sibik, J.; Zeitler, J.A.; Kidambi, P.R.; Hofmann, S.; Beere, H.E.; Ritchie, D.A. Low-bias terahertz amplitude modulator based on split-ring resonators and graphene. *ACS Nano* **2014**, *8*, 2548–2554. [[CrossRef](#)]
18. Grande, M.; Vincenti, M.A.; Stomeo, T.; Bianco, G.V.; de Ceglia, D.; Aközbeke, N.; Petruzzelli, V.; Bruno, G.; De Vittorio, M.; Scalora, M.; et al. Graphene-based perfect optical absorbers harnessing guided mode resonances. *Opt. Express* **2015**, *23*, 21032–21042. [[CrossRef](#)]
19. Liu, B.; Yu, W.J.; Yan, Z.D.; Tang, C.J.; Chen, J.; Gu, P.; Liu, Z.Q.; Huang, Z. Ultra-narrowband light absorption enhancement of monolayer graphene from waveguide mode. *Opt. Express* **2020**, *28*, 24908–24917. [[CrossRef](#)] [[PubMed](#)]
20. Amin, M.; Farhat, M.; Bağcı, H. A dynamically reconfigurable Fano metamaterial through graphene tuning for switching and sensing applications. *Sci. Rep.* **2013**, *3*, 2105. [[CrossRef](#)]
21. Lim, T.G.; Kim, T.Y.; Suk, J.W. Activated graphene deposited on porous Cu mesh for supercapacitors. *Nanomaterials* **2021**, *11*, 893. [[CrossRef](#)] [[PubMed](#)]
22. Furchi, M.; Urich, A.; Pospischil, A.; Lilley, G.; Unterrainer, K.; Detz, H.; Klang, P.; Andrews, A.M.; Schrenk, W.; Strasser, G.; et al. Microcavity-integrated graphene photodetector. *Nano Lett.* **2012**, *12*, 2773–2777. [[CrossRef](#)] [[PubMed](#)]
23. Cai, Y.J.; Guo, Y.B.; Zhou, Y.G.; Huang, X.D.; Yang, G.Q.; Zhu, J.F. Tunable dual-band terahertz absorber with all-dielectric configuration based on graphene. *Opt. Express* **2020**, *28*, 31524–31534. [[CrossRef](#)]
24. Jiang, X.Y.; Wang, T.; Xiao, S.Y.; Yan, X.C.; Cheng, L.E. Tunable ultra-high-efficiency light absorption of monolayer graphene using critical coupling with guided resonance. *Opt. Express* **2017**, *25*, 27028–27036. [[CrossRef](#)] [[PubMed](#)]
25. Lee, S.J.; Heo, H.J.; Kim, S. High fabrication-tolerant narrowband perfect graphene absorber based on guided-mode resonance in distributed Bragg reflector. *Sci. Rep.* **2019**, *9*, 4294. [[CrossRef](#)]
26. Long, Y.B.; Shen, L.; Xu, H.T.; Deng, H.D.; Li, Y.X. Achieving ultranarrow graphene perfect absorbers by exciting guided-mode resonance of one-dimensional photonic crystals. *Sci. Rep.* **2016**, *6*, 32312. [[CrossRef](#)]
27. Liu, F.; Chen, L.; Guo, Q.; Chen, J.; Zhao, X.; Shi, W. Enhanced graphene absorption and linewidth sharpening enabled by Fano-like geometric resonance at near-infrared wavelengths. *Opt. Express* **2015**, *23*, 21097–21106. [[CrossRef](#)]
28. Liao, Y.L.; Zhao, Y. Graphene-based tunable ultra-narrowband mid-infrared TE-polarization absorber. *Opt. Express* **2017**, *25*, 3208–32089. [[CrossRef](#)]
29. Yildirim, D.U.; Ghobadi, A.; Ozbay, E. Near-absolute polarization insensitivity in graphene based ultra-narrowband perfect visible light absorber. *Sci. Rep.* **2018**, *8*, 15210. [[CrossRef](#)]
30. Caridad, J.M.; Winters, S.; McCloskey, D.; Duesberg, G.S.; Donegan, J.F.; Krstić, V. Control of the plasmonic near-field in metallic nanohelices. *Nanotechnology* **2018**, *29*, 325204. [[CrossRef](#)]
31. Chen, J.H.; Jang, C.; Xiao, S.; Ishigami, M.; Fuhrer, M.S. Intrinsic and extrinsic performance limits of graphene devices on SiO₂. *Nature Nanotech.* **2008**, *3*, 206–209. [[CrossRef](#)]
32. Whelan, P.R.; Shen, Q.; Zhou, B.B.; Serrano, I.G.; Kamalakar, M.V.; Mackenzie, D.M.A.; Ji, J.; Huang, D.P.; Shi, H.F.; Luo, D. Fermi velocity renormalization in graphene probed by terahertz time-domain spectroscopy. *2D Mater.* **2020**, *7*, 035009. [[CrossRef](#)]
33. Li, Q.; Wang, T.; Su, Y.K.; Yan, M.; Qiu, M. Coupled mode theory analysis of mode-splitting in coupled cavity system. *Opt. Express* **2010**, *18*, 8367–8382. [[CrossRef](#)]
34. Piper, J.R.; Fan, S. Total absorption in a graphene monolayer in the optical regime by critical coupling with a photonic crystal guided resonance. *ACS Photonics* **2014**, *1*, 347–353. [[CrossRef](#)]
35. Thareja, V.; Kang, J.H.; Yuan, H.T.; Milaninia, K.M.; Hwang, H.Y.; Cui, Y.; Kik, P.G.; Brongersma, M.L. Electrically tunable coherent optical absorption in graphene with ion gel. *Nano Lett.* **2015**, *15*, 1570–1576. [[CrossRef](#)]